Available online at www.sciencedirect.com
SCIENCE DIRECT
Applied Catalysis A: General 308 (2006) 161–171
APPLIED CATALYSIS A: GENERAL
www.elsevier.com/locate/apcata

Improvement in the catalytic performance of In-mordenite through preferential growth on metallic monoliths

Juan M. Zamaro, María A. Ulla, Eduardo E. Miró *

Instituto de Investigaciones en Catálisis y Petroquímica, INCAPE (FIQ, UNL-CONICET) Santiago del Estero 2829, 3000 Santa Fe, Argentina

Received 15 February 2006; received in revised form 12 April 2006; accepted 15 April 2006
Available online 22 May 2006

Abstract

This work explored different ways of obtaining metallic monoliths coated with mordenite by hydrothermal synthesis. The results demonstrate that while direct synthesis favored the growth of ZSM5 instead of mordenite, the mordenite structure could only be obtained after seeding the support with crystals. Secondary synthesis showed great flexibility and possibilities of achieving different coating properties. Seed size and concentration, agitation and number of synthesis runs could be manipulated in order to change the microstructural characteristics. In most cases, the mordenite coatings were dense, thin films with high intergrowth. Additionally, the orientation of the zeolite crystals was so privileged that the channels in the *b* direction were perpendicular to the support whereas the channels in the *c* direction were parallel to it. This preferential orientation could be the main reason for the improved NO_x SCR activity of the In-mordenite monoliths if compared to the powder catalysts.

Keywords: Mordenite; Hydrothermal synthesis; Metallic monolith; SCR of NO_x with CH_4

1. Introduction

Interest in zeolitic materials for environmental applications has considerably increased in recent years, consequently spurring research in areas such as selective reduction of NO_x [1,2], oxidation of volatile organic compounds [3] and adsorption of hydrocarbons [4]. Considering the usual conditions of high flows and the presence of particles in those processes, low pressure drop and good tolerance to plugging by dust are essential requisites leading to the use of catalytic monoliths [5,6]. Zeolite monoliths can be obtained either under the form of extrudates [7] in which the zeolitic material is used to manufacture the monolith, or by the deposition of the zeolite as a coating onto a honeycomb substrate.

The most common zeolite coating techniques are colloidal-coating and slurry-coating [8]. In order to avoid the use of a binder to increase stability [9], the in situ growth has been proposed [10]. The advantage of this method is that a stronger adhesion to the support can be achieved. The disadvantages are that it is considerably more complex than slurry-coating and that a dense layer can be formed with small intercrystalline pores in which diffusion limitations can occur. However, not only intercrystalline diffusion is important in catalytic environmental applications. Accessibility to the active sites within the zeolite framework could also strongly pose a limit to reaction velocity [11]. Hydrothermal synthesis can help in obtaining preferential orientations to favor the diffusion of reactants. For example, ZSM5 films consisting in intergrown crystals would have a greater accessibility for the SCR of NO_x compared with a random packing of the crystals [12].

A thorough, critical review was published by Tavolaro and Drioli [13] in which they addressed zeolite membrane structures obtained by different methods and their applications. They concluded that new strategies are necessary to obtain membranes with consistent and predictable properties. In this vein, Lai et al. [14] reported that different film microstructures and orientations can be obtained manipulating the local growth environment by seeding the support with zeolite nanoparticles and changing the seed concentration. They found that while synthesis composition and crystallization condition have a larger impact on the crystal grain morphology, the crystal habit is mostly dictated by the growth environment. However, Li

* Corresponding author. Tel.: +54 342 4536861; fax: +54 342 4536861.
E-mail address: emiro@fiqus.unl.edu.ar (E.E. Miró).

0926-860X/$ – see front matter
doi:10.1016/j.apcata.2006.04.008

et al. [15] demonstrated that the synthesis composition also affects the crystals orientation.

With respect to the supports, a variety of them have been used for the synthesis of zeolites, among them ceramic foams, metallic monoliths and ceramic monoliths [16–18]. Recently, Ulla et al. [19] obtained a mordenite film structure on a ceramic monolith in which the accessibility of gaseous molecules to the inner channels was improved by preserving the individuality of the synthesized crystals. The better accessibility was proven in kinetic diffusion experiments where water adsorption was continuously monitored.

For some applications, metallic substrates are preferred due to their higher mechanical resistance and thermal conductivity and because the possibility of thinner walls allows higher cell densities and lower pressure drop [17]. An additional advantage of metallic substrates is the easy way in which different, complicated forms adapted to a wide variety of problems and uses can be produced with them, for example, in catalytic microreactors [20].

The objectives of this work are to study different ways of obtaining mordenite films by hydrothermal synthesis onto a metallic substrate (FeCrAl alloy), to characterize their physical–chemistry properties, and to evaluate the catalytic performance of these systems for the selective reduction of NO_x with methane as a test reaction, by exchanging In as active material.

2. Experimental

2.1. Support preparation

Metallic monoliths were prepared from stainless steel (Goodfellow FeCrAl alloy (Fecralloy®)) flat and corrugated strips with a thickness of 50 μm. These overlapping strips were rolled and tied with stainless steel wire into a cylindrical monolithic structure (1.5 cm in diameter and 2 cm long) with sinusoidal channels (Fig. 1) [21]. Strips were also used to perform zeolitic growths and to characterize them adequately.

The supports were treated at 900 °C for 22 h [21] in order to generate a surface layer of alumina by segregation and oxidation of the Al incorporated to the steel. The aim was to obtain a rough surface able to efficiently retain seeded mordenite crystals.

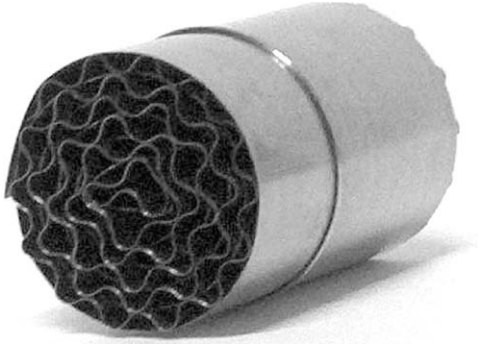

Fig. 1. FeCrAl stainless steel monolith. See Burgos et al. [21] for experimental details.

2.2. Hydrothermal synthesis

A synthesis gel of H_2O:SiO_2:Na_2O:Al_2O_3 = 80:1:0.38:0.025 composition was employed [19]. Colloidal SiO_2 (Ludox® AS 40), $Na_2Al_2O_4$ (Riedel-de-Haen) and NaOH (Cicarelli pro-analysis) were used as reactants. This gel was aged by stirring for 24 h at room temperature.

All the synthesis runs were conducted at 180 °C for 24 h. Direct and secondary synthesis runs were employed to obtain zeolitic growths. After every synthesis, the samples were sonicated for 10 min in an ultrasonic bath to remove weakly adhered material coming from the solution.

It should be remarked that no template agents were used in the procedure.

2.2.1. Direct synthesis

The support was vertically fixed inside a teflon vessel together with the aged synthesis gel, leaving a void of 2 cm. The vessel was transferred to an autoclave which was then placed in a stove for the hydrothermal treatment. After the treatment, the vessel was cooled, and the sample was withdrawn from the autoclave, washed in water, kept in an ultrasonic bath for 10 min to remove residues such as remains of grown material from the solution and finally dried at 120 °C for 4 h.

The remaining liquid phase from the synthesis was filtered and the crystals produced were recovered.

2.2.2. Secondary synthesis

The supports were seeded with mordenite crystals prior to the hydrothermal treatment. These seedings were carried out with two types of seeds. On the one hand, NH_4-mordenite zeolyst (Si/Al = 10) commercial crystals with a volumetric size distribution centered at 4 μm were employed. On the other, starting from those crystals, 200 nm seeds were fractioned by centrifuging at 3500 rpm for 20 min.

The seeding of strips and monoliths was performed by dipcoating in a suspension of the said seeds at 1 cm min^{-1}. Afterwards, the strips were dripped and dried in air for 30 min and then in a stove for 15 min (120 °C). The monoliths were softly blown with compressed air, prior to the drying. The seeding process was repeated twice. These seeded supports were subject to a hydrothermal treatment identical to the one performed during direct synthesis, and the crystals produced in solution were also recovered.

2.3. Indium incorporation

A synthesized NaMor/monolith was first exchanged with ammonium (80 °C, NO_3NH_4 1 M, 24 h). Then the NH_4Mor-coated monolith was loaded with In as the active phase for the SCR of NO_x with methane. The impregnation and exchange procedure was carried out with a 5 wt% solution of $In(NO_3)_3$ ($(NO_3)_3In{\cdot}5H_2O$ Aldrich). The impregnation procedure for powders is described elsewhere [22]. In this work, the NH_4Mor-coated monolith was immersed in the solution and the excess was blown, repeating this process until obtaining the desired loading (4% of indium). Between blowing steps, the monolith

was subsequently dried in a microwave oven and in a stove to obtain more uniform distributions of the indium precursor [8]. It was then calcined at 500 °C in air flow for 12 h to generate the In_2O_3 oxides and decompose the NH_4-zeolite in H-zeolite. Immediately after, the activation was carried out in air flow at 700 °C during 2 h in order to develop the $(InO)^+$ active sites by solid-state reaction between impregnated In_2O_3 and zeolite protons [23].

2.4. Characterization

2.4.1. Scanning electron microscopy (SEM)

The quality, orientation and crystalline microstructure of the mordenite film were examined with this technique. To do so, an SEM Jeol JSM-35C equipment was employed, operated at 20 kV acceleration voltages. The samples were glued to the sample holder with Ag painting and then coated with a thin layer of Au in order to improve the images.

2.4.2. Electron probe micro analysis (EPMA)

In order to study the distribution of the chemical elements present in the coating, a dispersive EDAX equipment coupled to the SEM was employed, with which the X-ray patterns coming from the sample were treated. The semiquantitative proportions of the elements were obtained by means of the SEMIQ method. The analysis was performed on a 1 μm strip on the coating cross-section from the interphase with the support up to the zeolite surface.

2.4.3. X-ray diffraction (XRD)

The zeolitic phase grown over the support and the crystals recovered from the solution were analyzed by XRD. The data obtained with this technique were also employed to perform the crystallographic preferential orientation (CPO) calculations on the coating, by means of the diffraction intensity ratio of selected crystalline planes. A Shimadzu XD-D1 equipment was used and the patterns were acquired at a scan rate of $2^\circ\ min^{-1}$ between $2\theta = 5^\circ$ and 40°. The sample was cut as a strip and placed on the edge of an aluminium sample holder window.

2.4.4. NO temperature-programmed desorption (NO TPD)

The nature of the interaction between the indium species and the NO molecule was studied with this technique. The desorbed NO_x were detected with an FTIR coupled to the outlet of a gas cell with calcium floride windows. The experiment was performed prior to the monolith catalytic test, and after purging in He flow ($50\ cm^3\ min^{-1}$) for 8 h at 400 °C. The monolith was then put in contact with a mixture of NO in He (5000 ppm) and left for 20 min. Afterwards, it was purged with He up to the total disappearance of NO from the gas phase. The programmed desorption was performed at $10\ °C\ min^{-1}$, during which the IR spectra were acquired.

2.4.5. Hg porosimetry

The meso and macroporous structure of the monolith coated with mordenite was studied by MIP. A Micromeritics Autopore 9220 V1.04 equipment was used operated between 0.1 and 350 bar.

2.4.6. Catalytic evaluation

The monolithic catalyst was evaluated for the SCR of NO_x with methane as a test reaction in a continuous flow system. The composition of the reacting stream was 1000 ppm NO, 1000 ppm CH_4 and 10% O_2, in He balance. The reaction was performed at atmospheric pressure, at temperatures between 300 and 650 °C, and at a $500\ cm^3\ min^{-1}\ g\ zeolite^{-1}$ total flow/zeolite loading ratio. The monolith was placed inside a quartz reactor between quartz wool plugs, and the free space between the monolith and the quartz tube was filled with CSi particles to avoid bypass flow. The gaseous mixtures were analyzed before and after reaction with an on-line FTIR Thermo Mattson Genesis II equipped with a gas analysis cell for the NO, NO_2 CO and CH_4 quantification. N_2O was not detected in the catalytic runs.

3. Results and discussion

3.1. Direct synthesis

The zeolite growth on the metallic surface obtained with this method was too low. The XRD analysis for the sample with growth showed the most important ZSM5 signals instead of the expected mordenite ones. Nevertheless, small incipient mordenite signals were also detected in some direct synthesis runs. Fig. 2b shows the XRD pattern obtained from the steel strip with the in situ crystalline growth.

The results indicate that, under the conditions described above and by direct synthesis, crystalline growths can be obtained mainly corresponding to ZSM5. Some mordenite was also generated, which was more pronounced in the crystals produced in solution where a mixture of both zeolites was present. This indicates that the nucleation and growth path towards the ZSM5 phase on the support is preferred over the mordenite one.

In all these experiments, the weight increase due to zeolite growth was low (about 1% p/p), and the weakness of the XRD signals obtained indicated poor development of the crystals. However, it should be stressed that this growth was obtained without employing any structuring agent.

Since with direct synthesis ZSM5 growth was obtained instead of mordenite, the secondary synthesis method with mordenite seeding was employed.

3.2. Secondary synthesis

One of the possibilities available for attempting the desired growth is to skip the nucleation stage by means of hydrothermal secondary synthesis. In this case, seeding with crystals from the desired zeolite avoids the limitations existing in the nucleation stage, and crystalline growth follows. To achieve this, the support was previously seeded with commercial modernite crystals and then subjected to hydrothermal treatment under similar conditions to those of direct

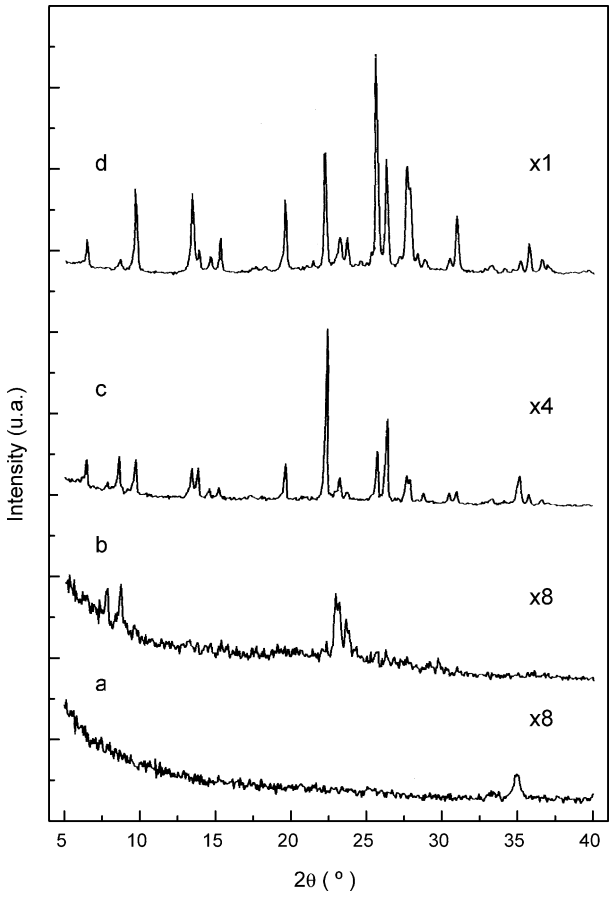

Fig. 2. XRD patterns: (a) Calcined support before synthesis, (b) Sample with coating obtained by direct synthesis, (c) Sample with mordenite coating obtained by secondary synthesis of microcrystals (Smi) and (d) Mordenite solution-recovered crystals.

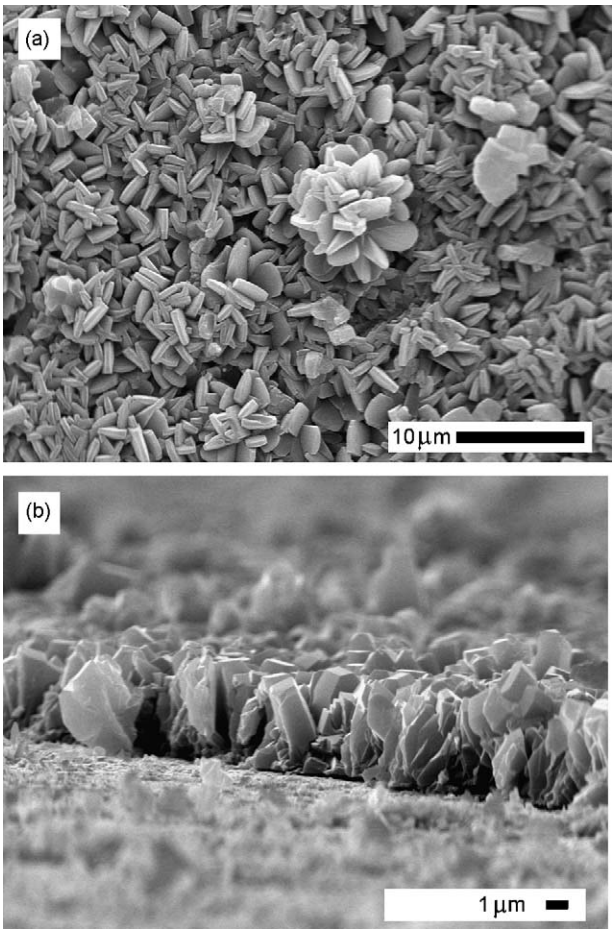

Fig. 3. SEM of mordenite coating obtained by secondary synthesis of microcrystals (Smi). (a) Top view and (b) Lateral view.

synthesis. Two seed sizes were used: micrometric and nanometric.

3.2.1. Micrometric seeding (Smi)

After the hydrothermal treatment, a considerably larger weight increase of the sample was observed (approximately 6%, p/p) if compared to direct synthesis. Through XRD, it could be observed that this weight increase corresponded to a mordenite crystalline growth, as shown in Fig. 2c. This same figure shows the patterns of the solution-recovered crystals (Fig. 2d).

Seeding with mordenite crystals prevented the synthesis to follow the path towards ZSM5 privileged by direct synthesis. The preferential spontaneous growth was redirected to that zeolite, avoiding the low mordenite nucleation given on the support. In turn, the growth kinetics of the mordenite nuclei was stronger than that of the ZSM5 nuclei that could have been produced. Through SEM (Fig. 3), it could be seen that the coating was a continuous film covering the whole surface of the support. These crystals were of prismatic morphology and vertically grown from the surface to the synthesis gel, as shown in Fig. 3b. A thickness of about 5 μm can be estimated. The crystals presented a slight intergrowth and in general, they preserved their identity. This same characteristic can be noticed in Fig. 3a where the intercrystalline spaces can be clearly seen.

3.2.2. Nanometric seeding (Sna)

In order to achieve a more uniform growth, smaller seeding crystals were considered more appropriate. Besides, taking into account how important the effect of seeding the support was in obtaining the coating, this variable was of interest. Initially, a suspension of 200 nm crystals with a 1.25 g lt^{-1}concentration was used. After hydrothermally treating the seeded support, a zeolite growth was obtained with an XRD analogous to that of direct synthesis. The low concentration of the suspension generated a scarce seed coating over the support. For this reason, during the hydrothermal treatment, both nucleation and ZSM5 growth were equally favored as in the unseeded case.

Afterwards, the concentration of the seeding suspension was increased by a factor of 4, by solvent evaporation. The support seeded with this suspension of 5 g lt^{-1} was analyzed by SEM; it was corroborated that the seeds were quite uniformly distributed, covering almost the whole surface with a monolayer. The support thus seeded was subject to synthesis under the same conditions as in the previous cases, and a mass increase was obtained similar to the one given with microcrystals, product of a mordenite crystal growth as determined by XRD (Fig. 4a).

It is concluded that a minimum seeding crystal concentration over the support is necessary for the synthesis to proceed to

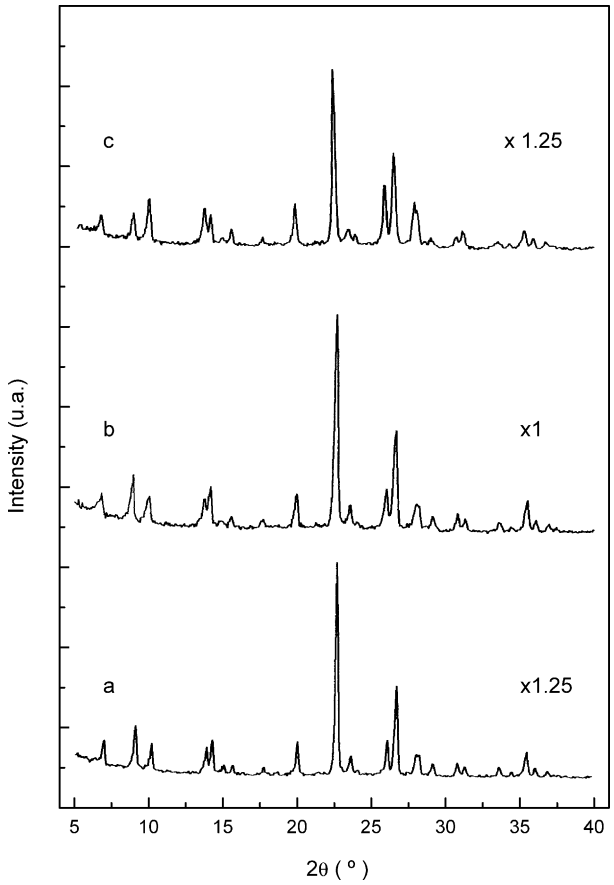

Fig. 4. XRD patterns: (a) Mordenite coating obtained with one hydrothermal synthesis, (b) Mordenite coating obtained with three hydrothermal treatments and (c) Mordenite coating obtained with agitation (Sna/stirr.).

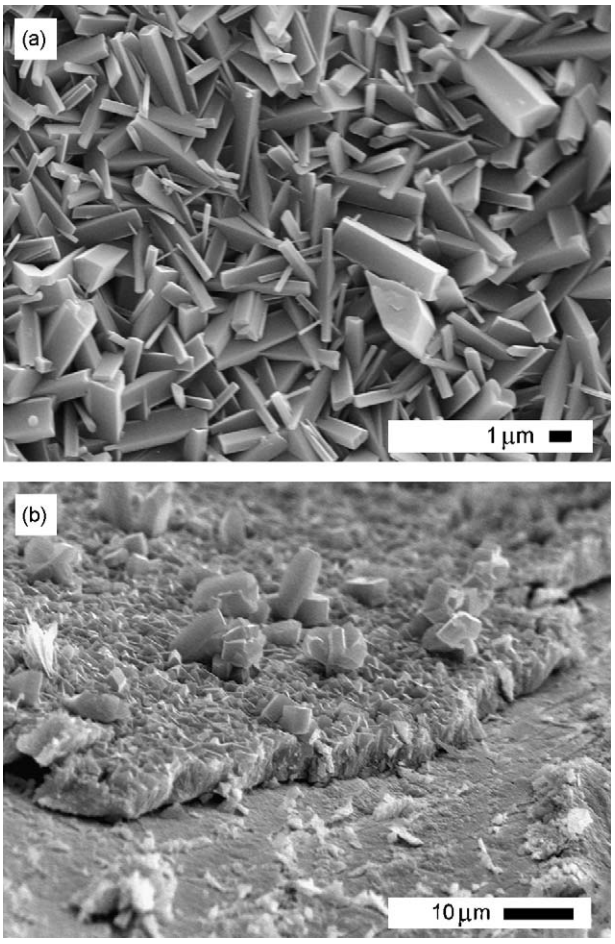

Fig. 5. SEM of mordenite coating obtained by secondary synthesis with nanocrystals (Sna). (a) Top view and (b) Lateral view.

mordenite. With lower concentrations, the spontaneous path towards ZSM5 prevails, showing again the higher nucleation rate for this zeolite.

The SEM images indicate a continuous growth formed by mordenite crystals with a microstructure different from that obtained by Smi. In the former case, the crystals exhibited a compressed prismatic shape (Fig. 5a) with a higher degree of intergrowth. A side view shows a coating thickness of 5 μm with a compact structure of intergrown crystals (Fig. 5b). This is similar to what has been reported in the literature for the case of mordenite films obtained over tubular alumina supports [15]. This image also shows some crystals grown on the top of the surface, maybe deposited after their nucleation in the liquid phase.

3.2.3. Nanometric seeding and consecutive syntheses (Snai; i = 1,2,3)

Tests of multiple crystalline growths over the support were performed so as to obtain a larger zeolite load and analyze whether this had an effect upon the coating crystallinity and structure. Thus, upon certain growths obtained by secondary synthesis of mordenite nanocrystals (Sna1), other consecutive syntheses runs were performed (Sna2 and Sna3). The first growth served as a source of nuclei for subsequent secondary growth. The increases in weight and thickness presented in Table 1 were obtained in these experiments.

The growths presented XRD signals characteristic of mordenite, which can be appreciated in Fig. 4a and b. The similarity of the diffraction patterns indicates that the crystalline characteristic of the coatings remained unchanged, retaining the mordenite phase. Through SEM (Fig. 6), it was observed that with a third synthesis the coatings presented an average thickness of about 15 μm, with a higher development of disordered surface growths in the shape of cumulus. The growth rate was approximately constant and ca. 0.2 μm h^{-1} during the subsequent growths.

In general, and despite the differences, the spatial location of the crystals on the support was maintained as well as their morphology, except for the modification introduced by the

Table 1
Characteristics of mordenite coatings obtained by secondary synthesis in consecutive hydrothermal treatments

Synthesis	Weight increases (%p/p)	Coating thickness (μm)
Sna1	6.1	5
Sna2	16.2	10
Sna3	25.9	15

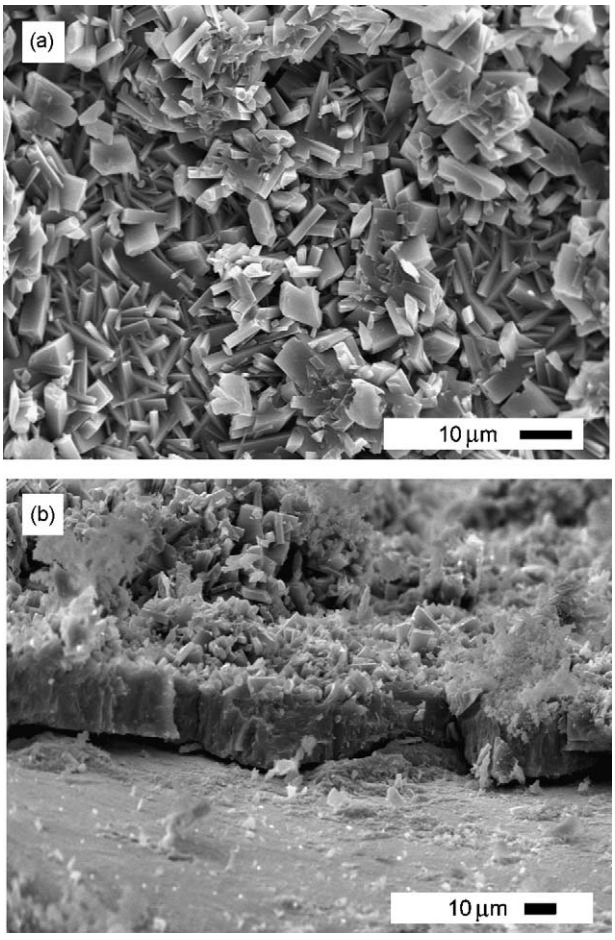

Fig. 6. SEM of mordenite coating obtained by secondary synthesis with nanocrystals and three hydrothermal treatments (Sna3). (a) Top view and (b) Lateral view.

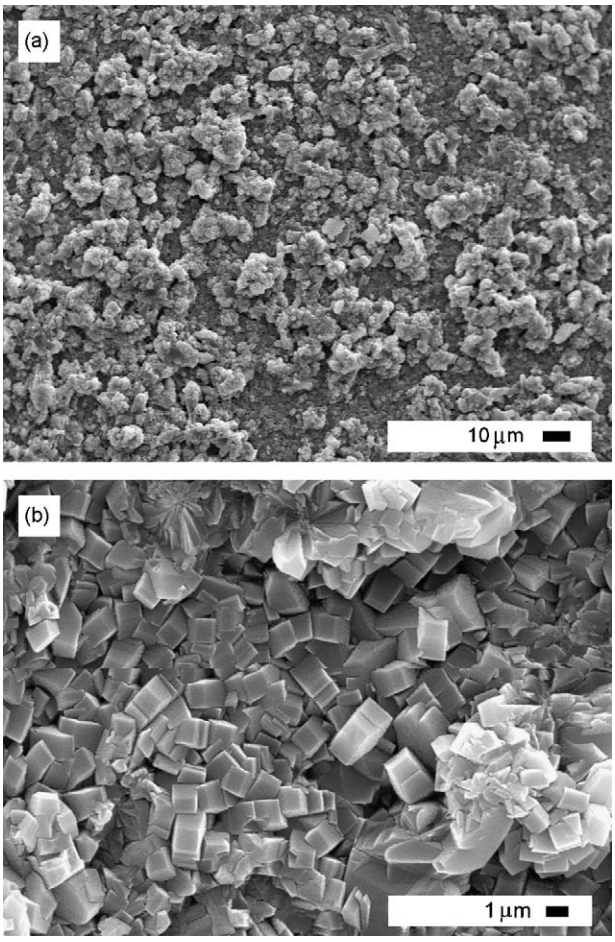

Fig. 7. SEM of mordenite coating obtained by secondary synthesis with nanocrystals and agitation (Sna/stir). (a) General top view and (b) Close-up top view.

crystalline cumulus. Subsequent growths took place starting from previously established crystals, which acted as nuclei from which the film kept growing. This was produced by maintaining a linear relation with synthesis time, even though with an increase in the number of disordered crystalline aggregates.

3.2.4. Nanometric seeding and synthesis with suspension stirring (Sna/sti)

Since these zeolitic coatings will be produced over monolithic structures, it may occur that the synthesis gel could find some diffusive limitation of the nutrient in the monolith channels. For this reason, it is of interest to study the effect of the synthesis gel stirring during the hydrothermal treatment. To do so, a secondary synthesis of nanocrystals seeded on metal strips was performed, placing the system under a 60 rpm agitation during the hydrothermal treatment. Under those conditions, a crystalline growth was obtained which, according to the XRD analysis, was constituted by mordenite crystals (Fig. 4c). The SEM images in Fig. 7 show that these crystals were placed on two levels over the support. On a lower plane, the prismatic crystals (of less compressed appearance) were located with their ends pointing to the synthesis gel, and above this plane, there were clusters of elevated cumulus. The dynamic synthesis conditions altered the coating morphology as regards the spatial location of the crystals. This structural difference could not only be observed by SEM but also in the XRD signals.

In all the growths obtained by secondary synthesis discussed so far, the XRD signals presented a modification of their relative intensities with respect to the different samples and also with respect to the powder crystals. This characteristic can be due to a preferential orientation of some particular crystalline plane and this led us to define an index to clearly characterize this aspect, denominated crystallographic preferential orientation (CPO) [24].

3.2.5. Crystallographic preferential orientation (CPO) calculations

In order to calculate this index, the ratios between the intensities of the XRD signals of selected crystallographic planes were considered. In this sense, those XRD signals presenting a greater intensity variation between the powder sample and the zeolite growth on the support were selected. Among these signals, the most appropriate ones were those coming from planes presenting very differentiated spatial

orientations, and whenever possible perpendicular to some crystallographic axis. Taking all these considerations into account, the X-ray diffractions from the following crystalline planes: [0 2 0] ($2\theta = 8.7$); [2 0 0] ($2\theta = 9.8$); [1 5 0] ($2\theta = 22.3$); [2 0 2] ($2\theta = 25.7$) were selected. The XRD signal intensities of the mordenite solution-recovered crystals were taken as references. The following CPO calculation expression was used:

$$\mathrm{CPO}\frac{x}{y} = \frac{(Is^x/Is^y) - (Ip^x/Ip^y)}{Is^x/Is^y}$$

where x and y represent the Miller indexes of the crystallographic planes, s indicates that they are the signals of the zeolite grown over the support, and p the powder zeolite signals. CPO indexes have been calculated in the open literature, but to the best of our knowledge only with respect to MFI coatings [25,26] and not mordenite.

With the selected crystallographic planes, the CPO (1 5 0)/(2 0 2) and CPO (0 2 0)/(2 0 0) indexes were defined. The first one indicates the magnitude of orientation of planes b against planes a and c, while the second offers a comparison between the orientation of plane b and that of plane a. In both cases, when these relations tend to zero the orientation of the crystallographic planes b approximates that existing in a powder sample, i.e., a random orientation. When the indexes tend to 1, the orientation of plane b is parallel to the support surface. And if the CPO takes negative values, they indicate the orientation of another plane different from b.

As indicated in Table 2, the CPOs have values close to one in all coatings, which shows a strong orientation of the crystallographic plane b in the growth parallel to the support surface. In general, all coatings were highly orientated, even though it was somehow lower in the coating obtained from synthesis under agitation and in consecutive synthesis. In the latter case, the images of the sample with three syntheses (Fig. 6) showed the existence of a great proportion of disordered crystalline cumulus above the ordered crystal layer. The same characteristic can be found in the sample obtained with stirring (Fig. 7). This must have been the reason behind the slight decrease in the global crystallographic orientation of these samples.

The crystallographic orientations obtained in the mordenite coatings, with axis b perpendicular to the surface of the stainless steel support imply that the great internal channels of the zeolite with c orientation were parallel to the surface of the support and the small channels in b, perpendicular to it. This orientation implies a faster crystal growth rate along axis b perpendicular to the support. Besides, the growth rates of axes a and c were also different. This difference in growth rate is shown in the crystal morphology since the crystals presented a compressed rectangular section.

Table 2
Crystallographic preferential orientation (CPO) values for the mordenite coatings

Sample	CPO [1 5 0]/[2 0 2]	CPO[0 2 0]/[2 0 0]
Smi	0.81	0.86
Sna1	0.90	0.91
Sna2	0.94	0.95
Sna3	0.80	–
Sna/stir	0.78	0.76

See Section 2 for calculations.

3.3. Structure and porosity of coated monoliths

The mordenite monolith obtained by secondary synthesis using nanocrystals as seeds (load 7% p/p) carried out under stirring conditions was characterized by MIP so as to determine the meso and macroporous structure of the monolith.

A very dense structure was determined, with a low total pore volume and a very small proportion of pores smaller than a micron, as shown by the accumulated intrusion curve in Fig. 8. On the other hand, at low intrusion pressures (in the right zone of the curve), the pore volume detected is due to the coating rugosity. The SEM images of the sample (Fig. 7) indicate no macropores but a high surface rugosity. Another important characteristic of the monolith was the almost total absence of intercrystalline spaces. This can be noticed from the plateau in the accumulated intrusion curve for sizes smaller than a micron and confirms that the coating consists in a continuous, dense zeolite film with a high degree of intergrowth, in agreement with the SEM micrographs. These growths presented a columnar structure. This characteristic is quite common in secondary growths of various zeolites. A possible explanation has been proposed by means of a competitive mechanism in which the faster crystal growth plane is being privileged during synthesis [27]. In this mechanism, the only crystals able to reach the surface are those whose highest growth rate coincides with the perpendicular direction to the support, thus generating a surface crystalline front with an elevated orientation. The crystals with the said axis deviated from normal will make contact with neighbouring crystals arresting their growth in that direction, remaining embedded in lower regions of the growth thickness. This phenomenon whose mechanism is not yet

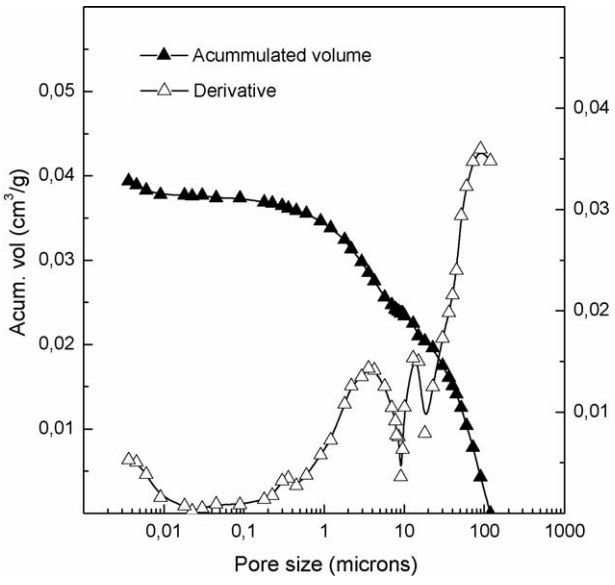

Fig. 8. Mercury intrusion porosimetry (MIP) of the mordenite coated monolith.

completely understood [15] is what causes intergrowth among crystals.

3.4. Chemical composition of the coatings

After the indium exchange, the elementary composition of the mordenite coatings was analyzed. EPMA analyses were performed to the cross-section, extracting information from the composition at different film depths. For each sector analyzed, a characteristic X-ray signal spectrum was obtained, showing the signals of all the elements present. These results expressed as a function of the coating depth were employed to build the EPMA profile portrayed in Fig. 9. In this figure, we can clearly see the existence of an aluminium enrichment in the zeolite coating, since on its surface the Si/Al ratio was 7.9. This value is lower than the theoretical value of the synthesis gel prepared with a ratio Si/Al = 20. This aluminium incorporation was produced from the support-zeolite interphase towards the coating outer surface. The abrupt initial increase of the Si/Al ratio from the support surface was due to the fact that the latter presented very little Si. Simultaneous to the incorporation of aluminium, some Fe and Cr is observed. As these latter elements were present only in the support, they undoubtedly migrated to the interior of the zeolite coating.

Fig. 9 also shows the profile of indium concentration which was almost increasing linearly to the surface. The value of the indium content on the surface was twice that of the zone close to the interphase (taken in reference to the Si signal which remained constant), even though the In/Al ratio increased more than twice as much due to the Al enrichment produced towards the growth surface. No indium was observed over the support below the interphase with the coating. This is logical, given the absence of porosity in the metallic material. The fact that In and Al distributions do not trace each other across the washcoat indicates that either not all the In is present as InO^+ in ion exchange sites or conversely some Al is present as extra-lattice alumina. The inhomogeneity in the In incorporation to the mordenite layer is due to the exchange procedure, which was accomplished by wet impregnation followed by reaction of In oxides with zeolite protons at high temperature (see Section 2).

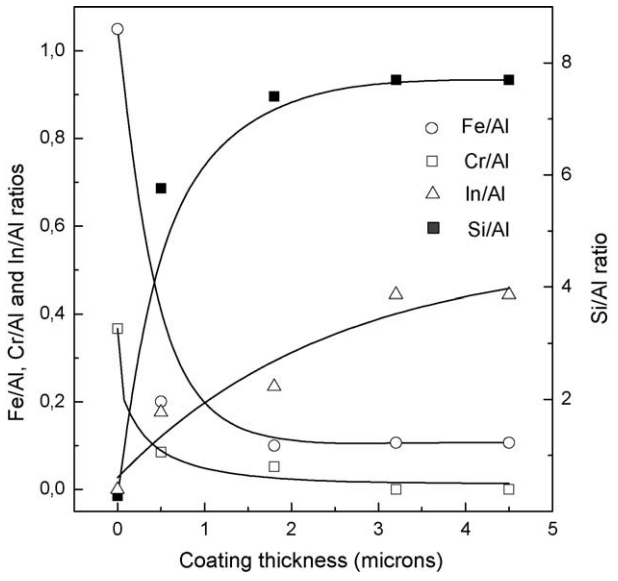

Fig. 9. EPMA profile of the In-mordenite monolith coating.

3.5. NO temperature-programmed desorption (TPD NO)

We observed that, after NO (He) adsorption at room temperature, and during the temperature increase, three main species desorbed: NO_2, NO and N_2O. It should be pointed out that we did not measure N_2. The main desorption signal was due to NO_2 desorption, N_2O was detected but only at trace levels. The preponderant desorption of the NO_2 species occured despite the fact that only NO was adsorbed. The experiment was repeated and the same result was obtained, which is shown in Fig. 10a.

These results suggest that NO disproportionated into N_2O and NO_2, and the N_2O formed decomposed further to N_2 and O_2, as reported by Li and Armor for the Cu-ZSM5 catalyst [28]. The difference is that on the Cu-containing catalyst, NO_2 decomposes to NO and O_2 before desorption, and in our system the NO_2 readily desorbs. In the cited work, they observed that fully oxidized catalysts favor NO_2 formation, thus suggesting that redox reactions take place during the adsorption–desorption processes. Indium-containing zeolite catalysts could present different In species: $(InO^+)\ Z^-$ at exchange positions (which are widely recognized as the active sites for the reaction under study); In_2O_3 crystals outside the zeolite channels, and In in the reduced state In^+Z^- [22]. Among these species, those that have more readily available oxygen are the active sites $(InO^+)Z^-$, suggesting that the TPD signals of NO_2 desorption could be related to these active sites. The NO desorption peak could be originated by NO adsorption on In_2O_3 species, which are not able to disproportionate NO molecules.

The NO_2 desorption was produced at two temperature zones: a sharp signal at low temperature (ca. 180 °C) and another peak at higher temperature (325 °C). Some NO desorption also occurred at low temperature (between 100 to 150 °C). By FTIR analysis using NO as probe molecule it was confirmed that the main adsorbed species in the In-mordenite is NO_2. This two NO_2 desorption signals could be assigned to InO^+ species with a different neighbourhood, but they are far apart in temperature (ca. 200 °C). It seems more plausible to envisage the formation of nitrates or nitrites and their subsequent decomposition to account for the high temperature NO_2 desorption.

By comparing with the TPD powder (Fig. 10b), the profile is similar even though the separation between NO_2 signals is greater in this case. Maybe these species in a slightly different environment or forming different intermediates with NO molecules could be related to the different catalytic behavior described in the next section.

3.6. SCR of NO_x with CH_4 on a InH-Mor/FeCrAl monolith

Abundant data are available in the literature for the NO SCR reaction with methane in the presence of excess oxygen using zeolite powder In-based catalysts [29,30]. The reaction results

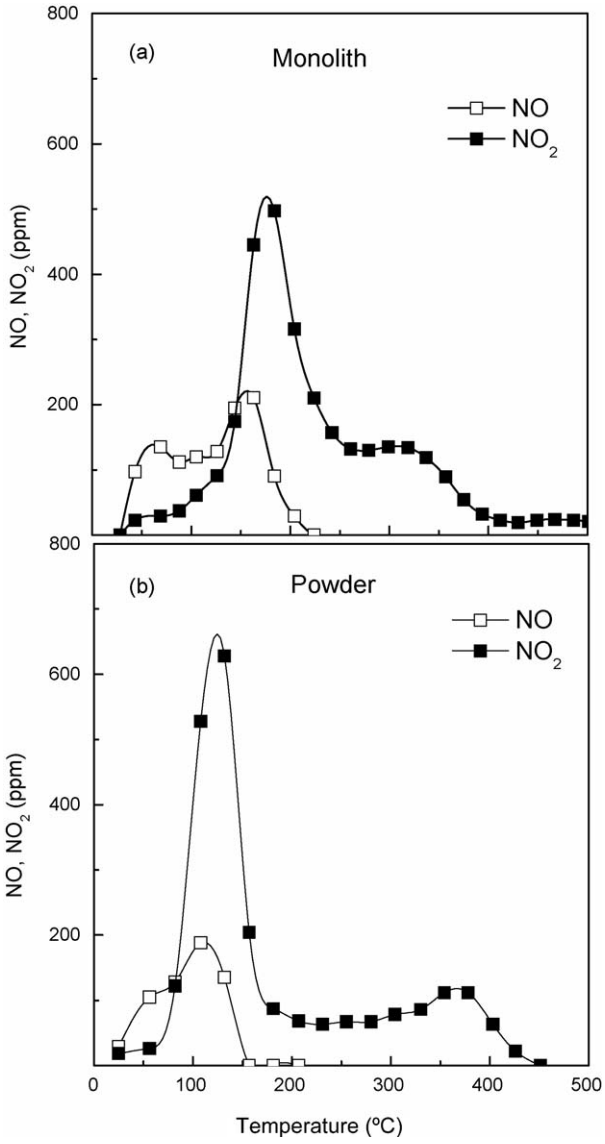

Fig. 10. NO TPD profile: (a) In-mordenite/FeCrAlloy monolith and (b) In-mordenite powder. See Section 2 for TPD conditions.

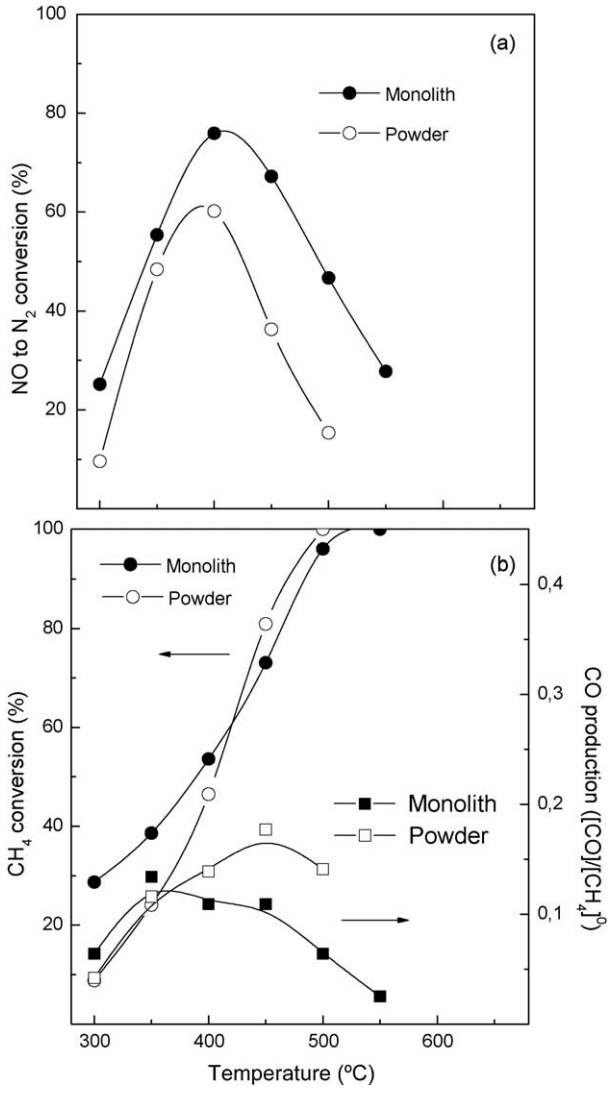

Fig. 11. Catalytic features of the In-mordenite monolith and powder: (a) NO to N_2 conversion and (b) CH_4 conversion and CO production. Reaction conditions: 1000 ppm of CH_4 and 1000 ppm of NO in He. Total flow to catalyst weight ratio: 500 cm^3/g.sec.

are provided to analyze the effect of monolithic catalyst properties on its catalytic performance. All the catalytic features of this monolith can be observed in Fig. 11. The most outstanding feature is that the activity was higher than that of the powder InH-Mor catalyst. Fig. 11a shows that the maximum conversion reached 76.5% at around 409 °C and maximum selectivity was also produced close to this temperature, even though it was slightly lower than that found for the powder. The production of CO in this metallic monolith, was lower than the powder catalyst mainly at high temperatures, although the maximum conversion temperature was similar.

The presence of iron in the zeolitic layer can justify the smaller production of CO for this monolith (Fig. 11b).

The higher activity of this monolith with respect to the powder cannot be attributed only to a more convenient NO_2 interaction with its active sites (TPD of NO). However, this characterization indicated a great proportion of InO^+ sites. If the NO_2 signals of the TPD characterization are considered to be originated by the InO^+ active sites both in the powder and the monolith, the TOF for both can be calculated. This TOF calculation made with the conversion obtained at 300 °C indicated a TOF monolith/TOF powder ratio = 3.

On the other hand, by EPMA analysis it was determined that indium and consequently the InO^+ sites in the monolith are concentrated on the coating surface. This location facilitates a greater accessibility of the reactants to the active sites. But also the accessibility of the InO^+ sites was also favored by the crystallographic orientation of the growth, which presented crystal axis *b* perpendicular to the support surface, as shown in Fig. 12. It means that the channels coinciding with the *b* axis of the mordenite were perpendicular to the metallic substrate whereas the mordenite channels in the *c* axis were parallel to it. This orderly disposition could have some advantage with respect to the random orientation of the powder. The entrance of reactant molecules could be through either of the two channels, directly through *c* and tangentially through *b*.

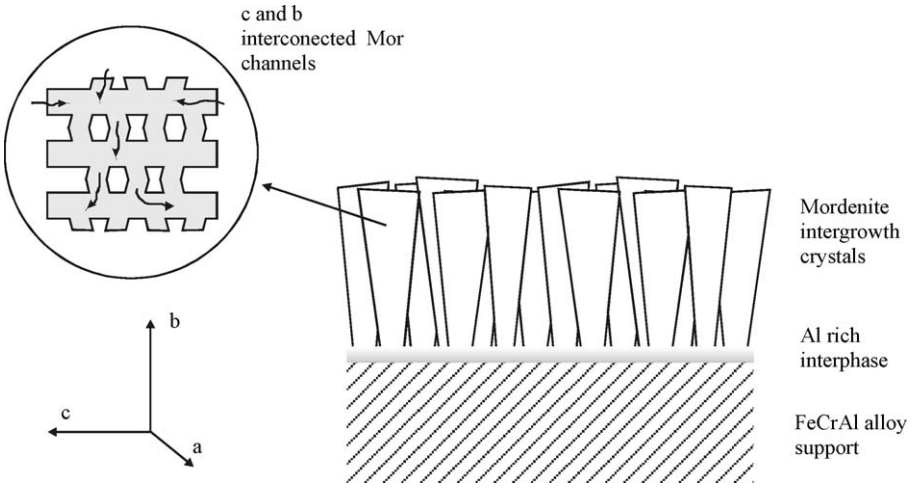

Fig. 12. Drawing of the zeolite growth structure illustrating the orientation of the channels relative to the surface and their accessibility to the gas phase.

In addition to the above considerations, the greater accessibility of the reaction gases to most of the active sites of the coating could also be benefited by the thinness of the latter (5 μm).

Finally, in order to investigate the effect of the presence of Fe and Cr, a metallic monolith coated with H-mordenite was catalytically evaluated. A very low activity was obtained (maximum conversion 14.5%), at high temperatures (550 °C) which was quite similar to the one reported for powder H-Mor catalysts evaluated under similar conditions [31], suggesting that Fe does not participate in the NO_x SCR reaction.

4. Conclusions

A monolithic In-mordenite catalyst was produced which presented a catalytic activity in the SCR of NO_x higher than that of the same powder catalyst. One of the main goals in catalyst structuring is to at least maintain the activity obtained with the powder. Obviously, this goal has not only been achieved but also surpassed. Results show that the secondary synthesis of this zeolite is a technique with great flexibility and possibilities of achieving different types of coatings. The microstructural characteristics of the coatings can be modified with seed size and concentration, agitation and number of synthesis runs. These growths were obtained without employing template agents, on flat stainless steel supports. The mordenite coating was a dense, thin film with high intergrowth, neither macro nor meso-porosity, surface rugosity, and microporosity typical of zeolite. The growth was enriched in Al, Fe and Cr in a lesser proportion, and the indium species accumulated close to the film surface. These species consisted in indium oxides such as In_2O_3 and InO^+ species exchanged in the zeolite network, which presented high interaction with the NO molecules in two differentiated neighbourhoods. A strong adherence of the zeolite film was achieved thanks to the merging of the alumina of the support in the interphase with the growth zeolite originating a homogeneous, continuous film. Being located on a stainless steel support constitutes and advantage for the coating given the excellent properties of this material such as mechanical resistance, heat transfer and design flexibility.

The outstanding characteristic of these coatings is their preferential crystallographic orientation on the *b* plane defining the zeolitic channels orientation. In this sense, the zeolitic channels in the *b* direction are perpendicular to the support while those in the *c* direction are parallel to it. The improvement in catalytic behavior can be related to certain factors that occur simultaneously such as a thin coating which minimizes diffusive limitations, and active phases preferentially located close to the surface, thus facilitating their interaction with the reacting molecules. Nonetheless, probably the main reason for this improvement is that the orientation of the mordenite crystals on the coating is advantageous. The *b*-axis, and therefore the mordenite *b*-channel, is homogeneously orientated perpendicular to the support along the zeolite coating. This fact, together with the crystal connections given by the *c*-channels, offers an open structure for the whole coating. The position of spatially oriented structured zeolites has not been given the attention it deserves in the field of catalysis. Its importance is well established only as regards the performance of zeolitic membranes concerning their permeation and separation properties.

The optimized design of monolithic reactors with environmental applications is important, and this includes the selection of type and quality of the support, the catalytic materials and the structural characteristics defined by the preparation method, in this case secondary synthesis. The results obtained will allow us to improve and develop mordenite metallic monoliths to be used in environmental catalysis.

Acknowledgements

The authors wish to acknowledge the financial support received from CONICET, ANPCyT and Banco Río-Universia 2004. Thanks are also given to Mario Montes from UPV, San Sebastián, Spain, for supplying the metallic monoliths, to Fabio Fontanarrosa from Ceride-Conicet for the SEM-EPMA analysis, and to Elsa Grimaldi for the English language editing.

References

[1] J.N. Armor, Catal. Today 26 (1995) 147.
[2] H. Hamada, Catal. Surv. Jpn. 1 (1997) 53.
[3] J. Bonacci, R. Farrauto, R. Heck, in: P. Cheremisinoff (Ed.), Encyclopedia of Environmental Control Technology, vol. 1, Tex. Gulf Publishing, Houston, 1998, p. 130.
[4] N.R. Burke, D.L. Trimm, R.F. Howe, Appl. Catal. B Environ. 4 (1) (2003) 97.
[5] R.M. Heck, S. Gulati, R.J. Farrauto, Chem. Eng. J. 82 (2001) 149.
[6] F. Kapteijn, T.A. Nijhuis, J.J. Heiszwolf, J.A. Moulijn, Catal. Today 66 (2001) 133.
[7] P. Avila, M. Montes, E.E. Miró, Chem. Eng. J. 109 (2005) 11.
[8] A.A. Nijhuis, A.E.W. Beers, T. Vergunst, I. Hoek, F. Kapteijn, J.A. Moulijn, Catal. Rev. Sci. Eng. 43 (4) (2001) 345.
[9] J.M. Zamaro, M.A. Ulla, E.E. Miró, Chem. Eng. J. 106 (2005) 25.
[10] R. Aiello, F. Crea, F. Testa, A. Spanti Gattuso, Stud. Surf. Sci. Catal. 125 (1999) 29.
[11] M.A. Ulla, R. Mallada, J. Coronas, L. Guitérrez, E. Miró, J. Santamaría, Appl. Catal. A Gen. 253 (1) (2003) 269.
[12] L. Li, B. Xue, J. Chen, N. Guan, F. Zhang, D. Liu, H. Feng, Appl. Catal. A Gen. 292 (2005) 312.
[13] A. Tavolaro, E. Drioli, Adv. Mater. 11 (12) (1999) 975.
[14] S.M. Lai, L.T.Y. Au, K.L. Yeung, Microporous Mesoporous Mater. 54 (2002) 63.
[15] G. Li, E. Kikuchi, M. Matsukata, Microporous Mesoporous Mater. 62 (2003) 211.
[16] G. Seijger, O. Oudshoorn, W. van Kooten, J. Jansen, H. van Bekkum, C. van den Bleek, H. Calis, Microporous Mesoporous Mater. 39 (2000) 195.
[17] N. Burgos, M. Paulis, M. Montes, J. Mater. Chem. 13 (2003) 1458.
[18] E.I. Basaldella, A. Kikot, C.E. Quincoces, M.G. Gonzalez, Mater. Lett. 51 (2001) 289.
[19] M.A. Ulla, E. Miró, R. Mallada, J. Coronas, J. Santamaría, Chem. Commun. (2004) 528.
[20] G. Kolb, R. Zapf, V. Hessel, H. Löwe, Appl. Catal. A Gen. 277 (2004) 155.
[21] N.B. García, Tesis Doctoral, UPV (2002).
[22] E.E. Miró, L. Gutierrez, J.M. Ramallo López, F.G. Requejo, J. Catal. 188 (1999) 375.
[23] M. Ogura, T. Ohsaki, E. Kikuchi, Microporous Mesoporous Mater. 21 (1998) 533.
[24] J.P. Verduijn, A.J. Bons, M.H. Anthonis, L.H. Czarnetzki, Int. Pat. Appl. PCT WO 96/01683.
[25] J. Hedlund, S. Mintova, J. Sterte, Microporous Mesoporous Mater. 28 (1999) 185.
[26] S. Mintova, J. Hedlund, V. Valtchev, B.J. Schoeman, J. Sterte, J. Mater. Chem. 8 (10) (1998) 2217.
[27] G. Li, X. Lin, E. Kikuchi, M. Matsukata, Stud. Surf. Sci. Catal. 135 (2001) 3153.
[28] Y. Li, J.N. Armor, Appl. Catal. 76 (1991) L2.
[29] E. Kikuchi, M. Ogura, N. Aratani, Y. Sugiura, S. Hiromoto, K. Yogo, Catal. Today 27 (1996) 35.
[30] M. Ogura, M. Hayashi, E. Kikuchi, Catal. Today 42 (1998) 159.
[31] A. Ribotta, M. Lezcano, M. Kurgansky, E. Miró, E. Lombardo, J. Petunchi, Catal. Lett. 49 (1997) 77.